www.ptcer.pl/mccm

MATERIAŁY CERAMICZNE /CERAMIC MATERIALS/, 62, 4, (2010), 533-539

Alumina-YAG Micro-Nanocomposites: Elaboration and Mechanical Characterization

P. Palmero[1]*, F. Lomello[1], G. Fantozzi[2], G. Bonnefont[2]

[1] Dipartimento di Scienza dei Materiali e Ingegneria Chimica, Politecnico di Torino, INSTM, R.U. PoliTO, LINCE Lab., C.so Duca degli Abruzzi 24, 10129 Torino, Italy
[2] Université de Lyon, INSA de Lyon, MATEIS UMR CNRS 5510, Bât. Blaise Pascal 7 Av. Jean Capelle, 69621 Villeurbanne, France
*e-mail: paola.palmero@polito.it

Abstract

A surface doping of commercial alpha alumina powders was performed to develop Al_2O_3 - 5 vol.% YAG ($Y_3Al_5O_{12}$) composites made by micronic or highly sub-micronic alumina particles and very fine YAG grains, yielded on the alumina surface by *in-situ* reaction.

In fact, the alumina powders were firstly dispersed in the aqueous suspension by ball-milling for different times as a function of the starting raw material and then an yttrium chloride solution was added as a precursor. After a controlled drying carried out by atomization, the modified powders were treated up to 1500ºC, following the phase development by XRD. Using these results, a suitable powder pre-treatment was selected; in particular, a flash heating by soaking the powders in a furnace kept in the range 1050-1150ºC was set up to control yttrium-aluminates crystallization and crystallite growth.

After that, green bodies were prepared by uniaxial pressing of dried powders as well as by slip-casting of slurries having a proper solid content. Pressureless sintering was optimized by the dilatometric study up to 1500ºC for 3 h. Less-conventional sintering routes, such as hot-pressing and spark plasma sintering, were also employed. The fired microstructures obtained by conventional or non-conventional densification routes were compared by SEM characterization. Finally, the sintered materials were submitted to a standard mechanical characterization (hardness and fracture toughness) in order to define the relationship between micro-nanostructural features and mechanical behaviour.

Keywords: Al_2O_3, YAG, Nanocomposite

MIKRO-NANOKOMPOZYTY TLENEK GLINU – YAG: WYTWARZANIE I CHARAKTERYSTYKA MECHANICZNA

Przeprowadzono domieszkowanie powierzchniowe handlowych proszków tlenku glinu odmiany alfa w celu opracowania kompozytów Al_2O_3 – 5 % obj. YAG ($Y_3Al_5O_{12}$) wytworzonych z mikronowych i mocno submikronowych cząstek tlenku glinu i bardzo drobnych ziaren YAG, osadzonych na powierzchni tlenku glinu drogą reakcji *in-situ*.

I tak, proszki tlenku glinu najpierw rozpraszano w zawiesinie wodnej drogą mielenia w młynie kulowym z zastosowaniem różnych czasów w zależności od wyjściowego materiału, a następnie dodawano w roli prekursora roztwór chlorku itru(III). Po kontrolowanym suszeniu, przeprowadzonym drogą rozpylania, zmodyfikowane proszki ogrzewano aż do 1500ºC i określano skład fazowy za pomocą metody XRD. Wykorzystując te wyniki wybrano odpowiednie warunku obróbki wstępnej proszku, a w szczególności ustalono sposób błyskawicznego ogrzewania polegającego na przetrzymaniu proszków w piecu o temperaturze z zakresu 1050-1150ºC, aby kontrolować krystalizację glinianów itru i wzrost krystalitów.

Potem, przygotowano surowe próbki drogą prasowania jednoosiowego proszków wysuszonych, a także drogą odlewania gęstw o odpowiedniej zawartości cząstek stałych. Wykorzystując badania dylatometryczne zoptymalizowano warunki spiekania swobodnego aż na 1500ºC przez 3 h. Zastosowano również mniej konwencjonalne drogi spiekania, takie jak prasowanie na gorąco i spiekanie plazmowe iskrą elektryczną. Mikrostruktury wypalonych tworzyw uzyskanych konwencjonalnym i niekonwencjonalnymi sposobami zagęszczania porównano za pomocą badań SEM. Na koniec, spieczone materiały poddano standardowej charakterystyce mechanicznej (twardość i odporność na pękanie), aby określić zależność pomiędzy cechami mikro-nanostrukturalnymi i zachowaniem mechanicznym.

Słowa kluczowe: Al_2O_3, YAG, nanokompozyt

1. Introduction

Many studies have been focused at the particulate-dispersed alumina composites, in order to improve both room and high temperature mechanical properties [1-4].

A suitable selection of reinforcing phases in alumina matrix can lead to several mechanical advances [5-6], through, first of all, proper microstructural modification. As an example, the suppression of grain growth and the control of grain morphology can be achieved by a pinning effect from the ultra-fine second phase particles. Enhanced creep behaviour can be also yielded thanks to the formation of strong interfaces between matrix and secondary phase [7-13]. In addition, if the reinforcing phase slightly differs in the thermal expansion coefficient from the matrix, thermal stresses at the grain boundaries can be induced, so that the

crack propagation can be modified [14] and, consequently, the material toughness improved. Fracture toughness can be also increased by many other mechanisms induced by the second phases, such as crack deflection, microcracking, grain bridging [4, 15-19]. In such a way, the tailoring of nano-microstructures can be performed, in order to obtain the desired mechanical properties.

Among the various ceramic reinforcing phases, yttrium aluminium garnet (YAG) has been recently exploited thanks to its excellent creep resistance, high melting point and quite a similar thermal expansion coefficient as alumina [13].

Alumina-YAG composites are frequently prepared by mechanical mixing, but this route does not allow an easy control of the 2nd phase particles distribution in the matrix [20]. For increasing the materials purity as well as the phase distribution homogeneity, wet-chemical syntheses are also applied, such as sol-gel [21-22] or co-precipitation of Y and Al ions from a water solution under controlled conditions [20, 23-25]. As an alternative route, alumina nanopowders have been doped with organic [11] as well as inorganic [26] yttrium salts, yielding highly homogeneous alumina-YAG nano-composites by the solid state reaction.

This paper discusses the processing of 95 vol.% Al_2O_3 – 5 vol.% YAG, by doping two commercial α-alumina powders, which mainly differ in the primary particle size. Green bodies are here prepared by uniaxial pressing and by slip casting and submitted to different densification routes (precisely, pressureless sintering, hot pressing and spark plasma sintering).

The aim of this work is to evaluate the main microstructural features, such as alumina and YAG sizes and their distribution in the fired composites, as a function of the raw powder, forming method and sintering route. Such information was coupled to some mechanical data (hardness and fracture toughness), with the aim of selecting the most promising microstructures for room as well as high-temperature applications.

2. Experimental

Two commercial alpha-alumina powders are employed for the development of alumina – 5 vol.% YAG composite materials.

The former, TM-DAR TAIMICRON, supplied by Taimei Chemical Co., Japan, is characterized by a mean grain size of about 150 nm and specific surface area of 14.5 m^2/g [27].

The latter, CR1 alumina powder supplied by Baikowski [28], France, is characterized by a higher average particle size of 0.6 μm and a lower specific surface area of 3 m^2/g. In Fig. 1, the raw powders morphology is presented.

The as-received powders were submitted to laser granulometry (Fritzsch Analysette 22 compact), evidencing a significant agglomeration for both materials.

In order to reduce the starting agglomerate size, the powders were ball-milled in pure distilled water, at solid contents of 33 wt%, by using a powder/spheres ratio of 1:10. Dispersion was carried out for 3 and 113 h for TM-DAR and CR1 powders, respectively.

Then, aqueous solutions of $YCl_3 \cdot 6H_2O$ (Sigma-Aldrich, 99.99 % purity) were prepared and added to the dispersed TM-DAR and CR1 slurries. The obtained doped suspensions were maintained under magnetic stirring for 2 h before drying, then diluted to 4 wt% and spray-dried (Bücher Mini Spray Dryer B-290).

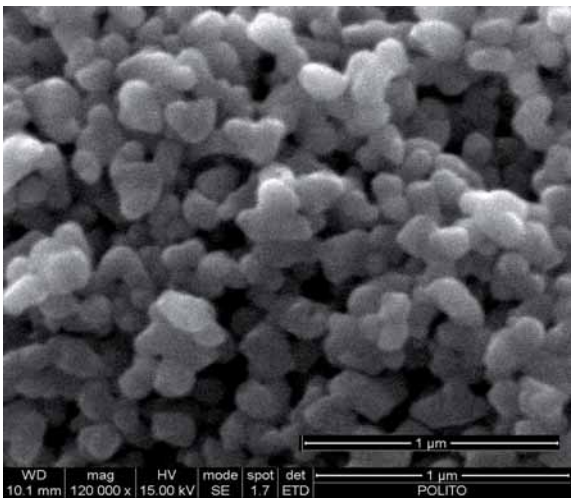

a)

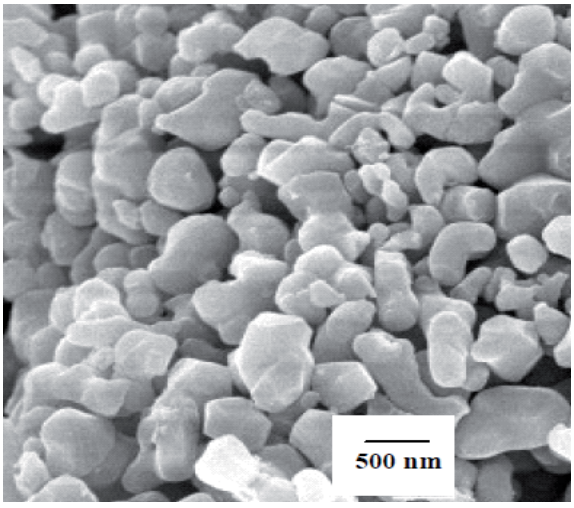

b)

Fig. 1. SEM micrographs of alpha-alumina powders: a) as-received TM-DAR and b) CR1.

Doped powders were calcined at various temperatures for different times and submitted to X-ray diffraction analysis (XRD, Philips PW 1710). On the ground of these results, "flash" calcinations, at 1150ºC for TM-DAR and 1050ºC for CR1, were respectively performed, by plunging the powders into a tubular furnace kept at a fixed temperature for a short time of 3 min. These fast treatments were carried out in order to minimize the crystallites growth and the aggregates formation during heating.

The doped, calcined powders are hereafter referred to as Y-TM and Y-CR, respectively.

After calcination, powder suspensions were prepared (with solid loading of 50 wt%) and ball-milled for 24 h. When dispersed, the suspensions were cast into suitable slip-casting (SC) moulds or dried in a oven to be uniaxially pressed (P) in pellets, followed by natural sintering (NS), hot pressing (HP) and spark plasma sintering (SPS).

In particular, NS was performed up to 1500ºC for 3 h (heating rate of 10ºC/min. up to 1100ºC and then 2ºC/min. up to 1500ºC); HP was carried out up to 1450ºC for 1 h (heating rate of 10ºC/min up to 1100ºC and 2 then ºC/min

up to 1450ºC; applied pressure of 80 MPa); pellets of 20 or 40 mm of diameter were sintered by SPS by heating up to 1350ºC (for Y-TM) and at 1450ºC (for Y-CR), under the applied pressure of 75 MPa.

The green densities were calculated from weight and geometrical measurements. Fired densities were measured by the Archimedes method. For microstructural observations, performed by scanning electron microscopy (SEM, Hitachi S2300) and environmental scanning electron microscopy (FEI XL 30 ESEM FEG), the samples were polished using diamond paste up to 1 μm, and then thermally etched at 1200ºC for 8 h.

In Fig. 2a schematic flow-chart of the elaboration process is reported, together with the samples designations as a function of the raw alumina powders, and the forming method.

Vickers hardness (HV) measurements were carried out on the sintered samples by using Tester FV-7. Indentations were made on polished surfaces with a load of 98.1 N (10 kG) held for 10 s; values are an average over five measurements. Fracture toughness was estimated using the Anstis' formula [28]. The impulse excitation technique allows the Young's modulus to be assessed. The tests were performed according to the ASTM standards C1259-01.

3. Results and discussion

3.1. Powders characterization

In Fig. 3, the cumulative size distributions of the as-received and dispersed TM-DAR (Fig. 3a) and CR1(Fig. 3b) powders are collected.

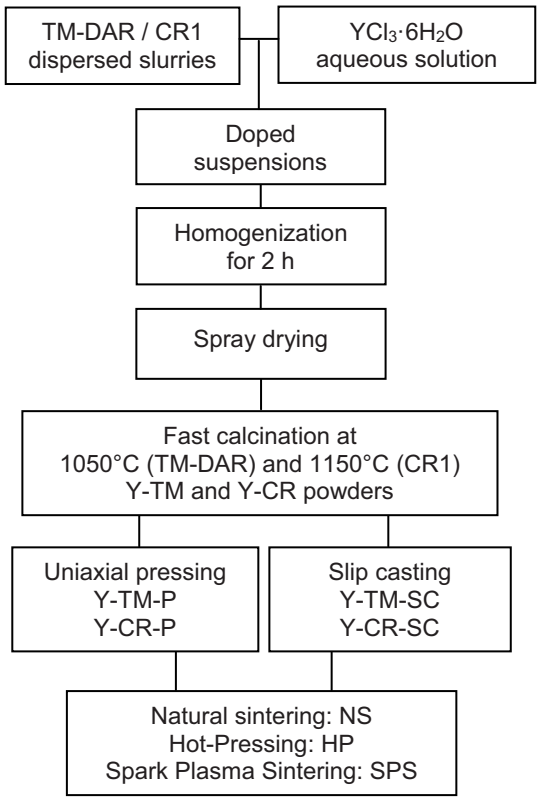

Fig. 2. Flow-chart of the elaboration process with samples designation as a function of the raw alumina powders and forming methods. Designation for the sintering routes are also reported.

In both cases, a significant reduction of the starting agglomerate size was determined after dispersion. In fact, sizes of 0.43, 4.46 and 16.88 μm, corresponding to 10 (d_{10}), 50 (d_{50}) and 90 % (d_{90}) of the cumulative volume distribution, were observed in the as-received TM-DAR. After dispersion, these values were reduced to 0.27, 0.53 and 1.12 μm, respectively.

The starting CR1 powder was agglomerated in a larger extent, since d_{10}, d_{50} and d_{90} values were 4.1, 13.4 and 32.7 μm, respectively. After a prolonged ball-milling, the above values decreased to 0.44, 0.81 and 1.37 μm.

In Fig. 4, the XRD patterns of Y-TM and Y-CR are reported. The materials significantly differ in crystallization behaviour. In fact, Y-TM "flash" heated at 1150ºC for 3 min shows traces of orthorhombic perovskite $YAlO_3$ (JCPDF N° 70-1677, YAP) near α-alumina (JCPDF N° 461212) (curve I); in contrast, pure YAG (JCPDF N° 33-0040) crystallized near α-Al_2O_3 in Y-CR. For a sake of clarity, in Fig. 4, only the peaks in the 22-50º 2θ range are reported.

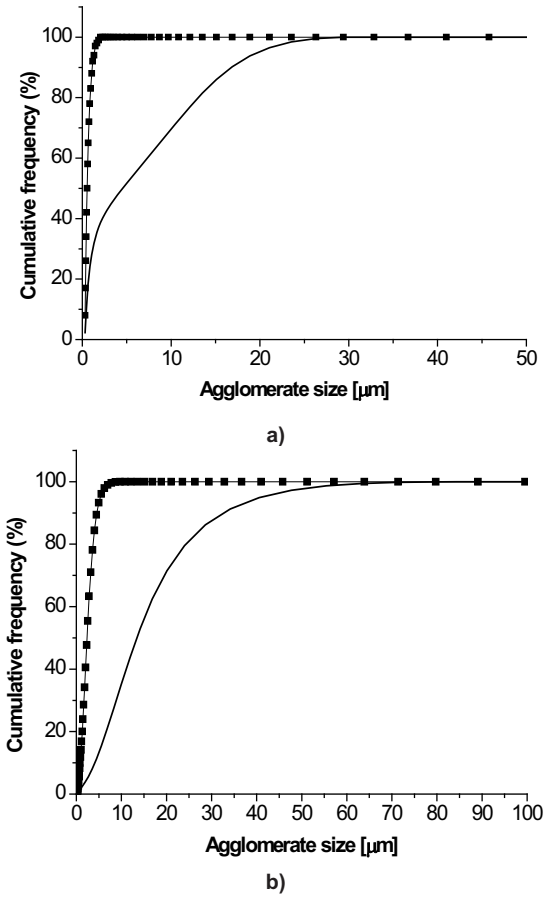

Fig. 3. Cumulative size distribution by volume of the as-received (solid line) and dispersed (squares) powders: a) TM-DAR and b) CR1.

In the former case, the XRD intensity of YAP increased by increasing the calcination temperature up to 1250ºC; however, starting from 1220ºC, also YAG crystallized. After the high-temperature calcination (1500ºC for 3 h), a composite powder made of pure YAG and α–Al_2O_3 was yielded in both cases (see Fig. 5 for Y-TM).

3.2. Forming and sintering

Y-TM and Y-CR were uniaxially pressed in bars at 350 MPa and submitted to dilatometric analysis (samples

labelled as Y-TM-P and Y-CR-P). The green bodies reached similar densities, precisely of 2.29 g/cm^3 for Y-TM-P and 2.25 g/cm^3 for Y-CR-P.

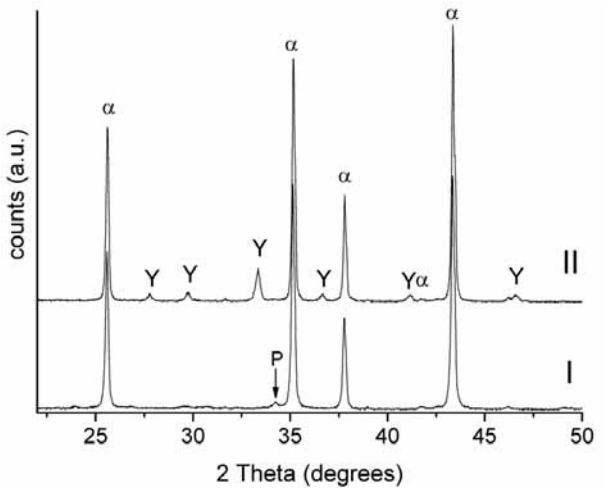

Fig. 4. XRD patterns in the 22-50° 2θ of Y-TM "flash" heated at 1150ºC for 3 min (I) and of Y-CR "flash" heated at 1050ºC for 3 min (II) (α = α-Al_2O_3, Y = YAG, P = orthorhombic $YAlO_3$).

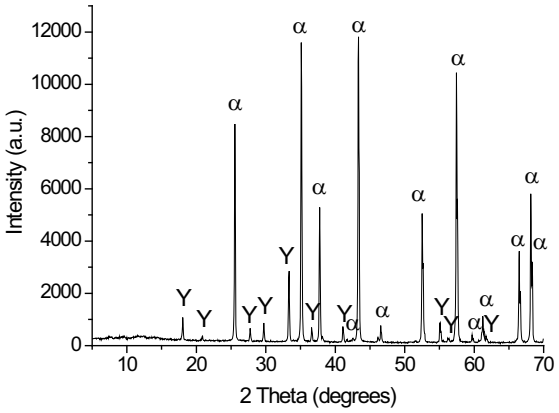

Fig. 5. XRD pattern of Y-TM calcined at 1500ºC for 3 h (α= α-Al_2O_3, Y = YAG).

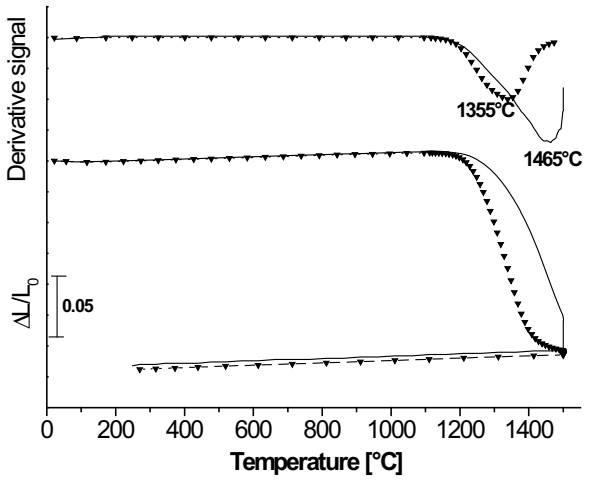

Fig. 6. Dilatometric and derivative curves of Y-TM-P (triangles) and Y-CR-P (solid line).

In Fig. 6, their dilatometric and derivative curves are compared. Linear shrinkages of 16.9 % and 16.4 % were respectively recorded for Y-TM-P (triangles) and Y-CR-P (solid line); the temperatures of maximum sintering rate (given by the derivative curves) were at 1335ºC and at 1465ºC, respectively. Fired densities of 97.52 % TD and 96.0 % TD were yielded for Y-TM-P and Y-CR-P samples.

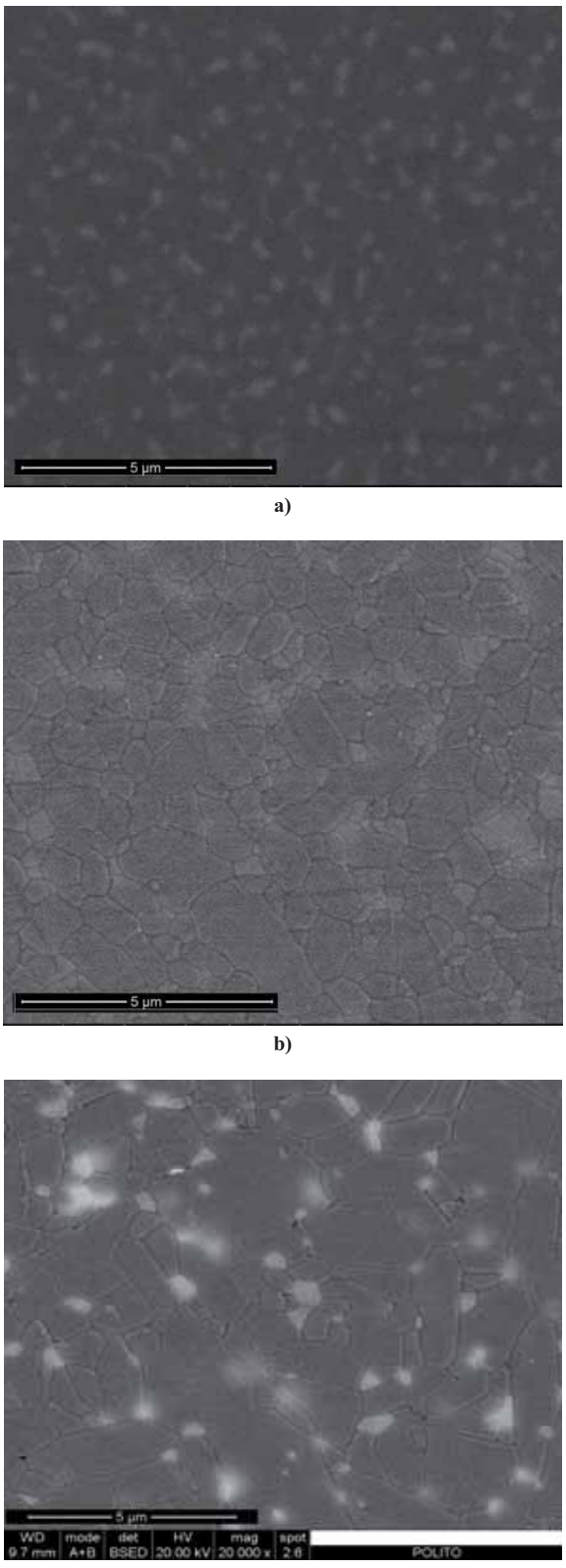

Fig. 7. SEM micrographs of Y-TM-SC and T-TM-P pressureless sintered at 1500ºC for 3 h: a) Y-TM-SC lower-magnification BSE image, b) Y-TM-SC higher-magnification SE image, c) Y-TM-P higher-magnification BSE image.

Trying to reach the full densification, slip cast samples (Y-TM-SC and Y-CR-SC) were also prepared and pressureless sintered in the above conditions. Their green densities were respectively 2.92 and 2.75 g/cm^3, significantly higher than those of the pressed samples, particularly for Y-TM-SC. This can be imputed to a better homogeneity and a higher degree of particle packing induced by the wet forming method. After sintering, Y-TM-SC reached almost theoretical density (99.7 % TD), while a poor value was still achieved by Y-CR-SC (94.4 % TD).

In Fig. 7, some SEM micrographs of Y-TM-SC (Figs. 7a and 7b) and Y-TM-P (Fig. 7c), pressureless sintered at 1500°C for 3 h, are compared.

The forming method seems not to affect significantly the phase distribution. In fact, a highly homogeneous distribution of YAG in the alumina matrix was present in both pressed and slip cast samples, as shown by the lower-magnification BSE image (Fig. 7a) for Y-TM-SC. A very dense microstructure was observed for Y-TM-SC (Fig. 7b), while some residual porosity was still present in Y-TM-P (Fig. 7c).

In both materials, the matrix was made of a mixture of micronic equiaxed and elongated alumina grains. The second phase was mainly located at alumina grain boundaries or triple points, and only a few inter-granular particles were found. The average YAG grain size was about 350 nm and 450 nm in Y-TM-SC and Y-TM-P, respectively.

In Fig. 8, the microstructures of Y-CR-SC and Y-CR-P are also presented. Also in this case, a highly homogeneous distribution of α-alumina and YAG particles was obtained in both slip cast and pressed samples. Similarly to the previous materials, YAG was prevalently located in an intergranular position with respect to the micronic alumina matrix. YAG mean size was about 650 nm and 400 nm in the slip cast and pressed samples, respectively. Differently from Y-TM samples, a more significant residual porosity was observed.

The same materials were also sintered by HP and SPS. When less conventional sintering routes were employed, it was possible to lower the maximum sintering temperatures in the range 1350-1450°C to reach almost theoretical densities (Table 1). In fact, HP was carried out at 1450°C for both Y-TM and Y-CR samples. In contrast, SPS was performed at 1350°C for Y-TM and 1450°C for Y-CR.

In the case of Y-TM, the fired densities of the slip cast samples were always slightly higher that those of the pressed materials, independently from the densification route.

In contrast, almost similar values were obtained in the case of Y-CR slip cast or pressed samples, denoting that for this material the forming method did not affect the final density in a significant way, as already observed in the case of pressureless sintered materials.

In Fig. 9, the microstructures of Y-TM-P densified by HP (Fig. 9a) and by SPS (Fig. 9b) are compared.

As expected, highly dense microstructures were obtained in both cases. In addition, if a reference to the pressureless sintered samples is made, overall finer microstructures were observed. A more remarkable difference was present in the case of the SPS process, as a result of the lower sintering temperature, and short soaking time in the high-temperature region and simultaneous application of pressure. In fact, the

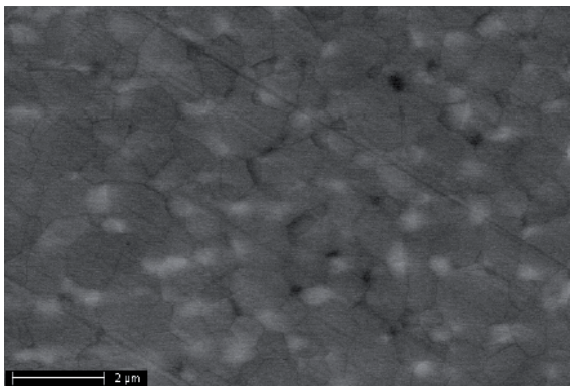

a)

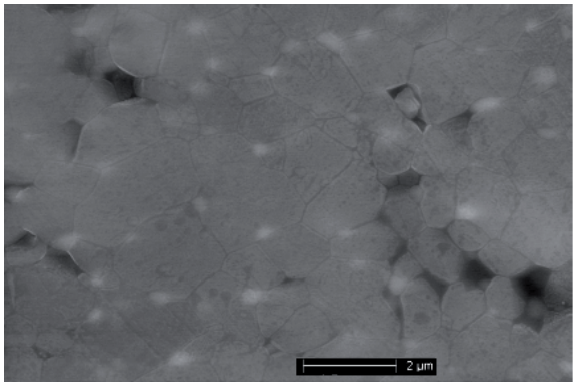

b)

Fig. 8. SEM micrographs of Y-CR-SC and Y-CR-P pressureless sintered at 1500°C for 3 h: a) Y-CR-SC BSE image, b) Y-CR-P BSE image.

average grain size of alumina and YAG grains was respectively 650 nm and 430 nm in hot-pressed Y-TM; the mean values of about 510 and 265 were indeed determined for the spark plasma sintered material.

The microstructure in Fig. 9b differs from the one already reported in literature [30] for a 90 vol.% alumina - 10 vol.% YAG composite material processed by SPS at 1300°C, in which YAG grains of about 500 nm were homogeneously distributed into the micronic alumina matrix.

In Fig. 9c, the fracture surface of Y-CR processed by SPS is presented. If compared to Y-TM sample sintered by the same route (Fig. 9b), the microstructure is less fine, since alumina and YAG phases reached a mean size of about 1 µm and 530 nm, respectively. This difference is probably a direct consequence of the starting primary size of the two alumina powders. In addition, this material reached an almost theoretical density only by increasing the maximum sintering temperature to 1450°C. Similar microstructural features were observed for hot pressed Y-CR.

3.3. Mechanical characterization

In Table 1, the hardness and fracture toughness values for all the fired specimens are collected.

Considering the Y-TM samples, the slip cast materials are harder than the pressed ones when pressureless sintered or hot-pressed, due to their higher final density. Moreover, the SPS processed materials achieved even higher hardness values, as expected by considering their very high final density and their significantly finer microstructure. As

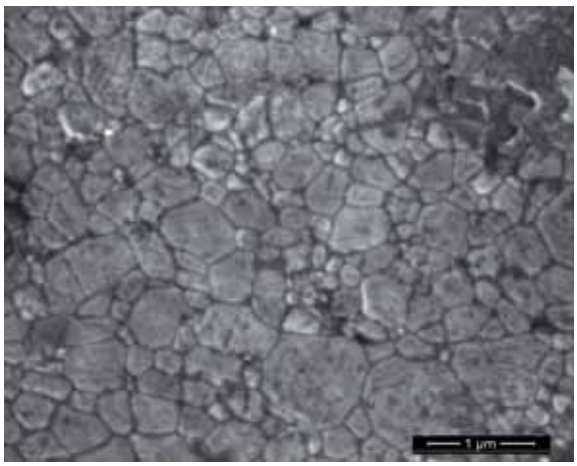

a)

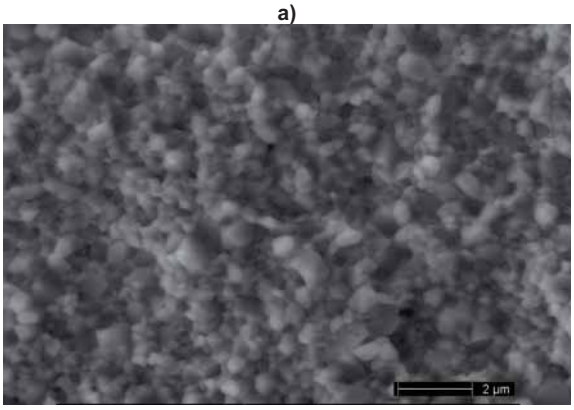

b)

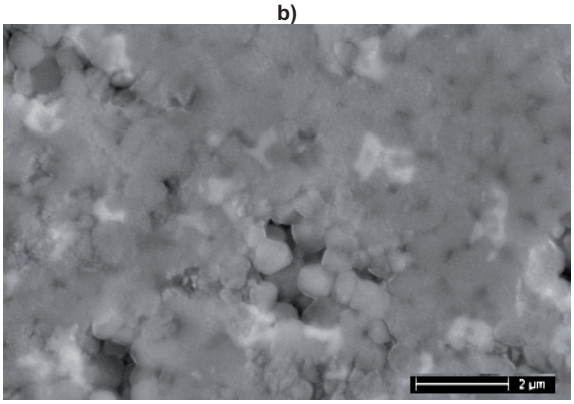

c)

Fig. 9. SEM micrographs of Y-TM-P sintered by a) HP, and b) SPS, c) SEM micrograph of Y-CR-P sintered by SPS.

a comparison, HV of 16.14 GPa was reported in literature for a completely dense alumina-25 vol.% YAG composite, made by a sub-micronic alumina matrix and a homogeneous distribution of fine (100-600 nm) YAG grains [23].

Considering the fracture toughness, the lower values were yielded by the pressureless sintered bodies. Less- conventional sintering routes led to tougher materials, especially in the case of the hot-pressed slip cast samples, whose K_{Ic} was closed to 7 MPa·m$^{1/2}$. The fracture path seemed to change from a rather intergranular to transgranular mode when HP and SPS sintered materials are concerned. However, this behaviour must be still confirmed by further investigations. As a comparison, fracture toughness in the range 3-5.8 MPa·m$^{1/2}$ was determined for YAG-reinforced alumina micro/nano-composites, with YAG phase contained in the 5–50 vol.% range [11, 18, 23].

Table 1. Fired density, Vickers Hardness and K_{Ic} values for slip cast (SC) and pressed (P) Y-TM bodies densified by pressureless sintering (NS), hot-pressing (HP) and spark plasma sintering (SPS).

Sintering route	Sample	Fired density [% TD]	Hardness [GPa]	K_{Ic} [MPa·m$^{1/2}$]
Y-TM				
NS-1500	SC	99.7	18.8 ± 1.13	4.42
NS-1500	P	97.5	16.3 ± 1.84	5.11
HP-1450	SC	99.8	19.8 ± 2.94	6.95
HP-1450	P	98.5	18.0 ± 0.88	6.21
SPS-1350	SC	99.5	19.1 ± 0.52	5.57
SPS-1350	P	99.4	19.9 ±0.50	5.82
Y-CR				
NS-1500	SC	94.4	18.7 ± 0.49	4.7
NS-1500	P	96.0	19.1 ± 1.73	7.12
HP-1450	SC	99.1	21.4 ± 1.71	6.03
HP-1450	P	98.9	19.7 ± 1.10	6.37
SPS-1450	SC	99.7	18.8 ± 0.81	7.32
SPS-1450	P	99.7	19 ± 0.64	7.32

If Y-CR materials are compared, their Vickers hardness was in the range 18.7-19.7 GPa, similarly to Y-TM materials, apart from Y-CR-SC, whose hardness was even higher (about 21 GPa).

Considering the fracture toughness, the higher values were found for the SPS materials. In the case of the pressureless sintered samples, a remarkable difference among the slip cast and pressed bodies was found, being Y-CR-P the tougher one. If reference to their microstructures (Fig. 8) is made, it can be supposed a more important toughening effect from the the finer YAG particles contained in the pressed material.

Also in this case, a more systematic investigation of the mechanical properties is necessary to understand their evolution as a function of processing methods and microstructural features.

Young's modulus of some representative composites, necessary to obtain the fracture toughness values, was measured by Grindosonic apparatus, yielding 419.2 GPa. As a comparison, the elastic modulus, given by the rule of mixtures, was also calculated (409.2 GPa), in a good agreement with the experimental value.

4. Conclusions

Surface doping of two commercial α-alumina powders (having primary particles size of about 150 and 600 nm) with an yttrium chloride aqueous solution has been successfully exploited to produce highly pure alumina – 5 vol.% YAG composite powders.

Green specimens obtained by uniaxial pressing as well as by slip casting were densified by conventional (pressureless sintering) and non-conventional (hot-pressing and

spark plasma sintering) routes. In the former case, only the samples obtained from the finer doped-alumina reached theoretical density. In contrast, non-conventional routes led to highly dense microstructures, independently from the starting alumina powder and the forming method.

In such a way, a wide range of obtainable micro-nanostructure is here shown, depending on the raw alumina powder, the forming method and the sintering route.

A basic mechanical characterization (in terms of Vickers hardness and fracture toughness) was carried out on all the densified materials, and data correlated with their main microstructural features.

The established correlation among process parameters and final microstructures will be exploited for a more effective micro-nanostructural tailoring of the composites, in order to obtain the desired mechanical properties.

As a future activity, the high-temperature mechanical characterizations will be also carried out on the best promising materials, selected on the ground of this preliminary investigation.

References

[1] Harmer M.P., Chan H.M., Miller G.A.: „Unique opportunities for microstructural engineering with duplex and laminar ceramic composites", J. Am. Ceram. Soc., 75, (1992), 1715-1728.

[2] Evans A.G.: „Perspective on the development of high-toughness ceramics", J. Am. Ceram. Soc., 73, (1990), 187-206.

[3] Jang B.K., Enoki M., Kishi T., Oh H.K.: „Effect of second phase on mechanical properties and toughening of Al_2O_3 based ceramic composite", Comp. Eng., 5, (1995), 1275-1286.

[4] Sternitzke M.: „Review: Structural ceramic nanocomposites", J. Eur. Ceram. Soc., 17, (1997), 1061-1082.

[5] Lange F.F., Hirlinger M.M.: „Hindrance of grain growth in Al_2O_3 by ZrO_2 inclusions", J. Am. Ceram. Soc., 67, (1984), 164-168.

[6] French J.D., Harmer M.P., Chan H.M., Miller G.A.: „Coarsening-resistant dual-phase interpenetrating microstructure", J. Am. Ceram. Soc., 73, (1990), 2508-2510.

[7] Lartigue S. and Prister L.: „Dislocation activity and differences between tensile and compressive creep of yttria doped alumina", Mater. Sci. Eng. A, 164, (1993), 211-215.

[8] French J.D., Zhao J., Harmer M.P., Chan H.M., Milller G.A.: 'Creep of duplex microstructures", J. Am. Ceram. Soc., 77, (1994), 2857-2865.

[9] Tai Q., Mocellin A.: „Review: High temperature deformation of Al_2O_3-based ceramic particle or whisker composites", Ceram. Int., 25, (1999), 395-408.

[10] Ohji T.: „Creep inhibition of ceramic/ceramic nanocomposites", Scripta Mater., 44, (2001), 2083-2086.

[11] M. Schehl, L.A. Díaz, R. Torrecillas: „Alumina nanocomposites from powder–alkoxide mixtures", Acta Mater., 50, (2002) 1125-1139.

[12] Sataptyh L.N., Chokshi A.H.: „Microstructural development and creep deformation in an alumina – 5 % yttrium aluminium garnet composite", J. Am. Ceram. Soc., 88, (2005), 2848-2854.

[13] Duong H., Wolfestine J.: „Creep behaviour of fine-grained two-phase Al_2O_3-$Y_3Al_5O_{12}$ materials", Mater. Sci. Eng. A, 172, (1993), 173-179.

[14] Choi S.M., Awaji H.: „Nanocomposites – a new material design concept", Sci. Tech. Adv. Mater., 6, (2005), 2-10.

[15] Jeang Y.K., Niihara K.: „Microstructure and mechanical properties of pressureless sintered Al_2O_3/SiC nanocomposites", Nanostruct. Mater., 9, (1997), 193-196.

[16] Derby B.: „Ceramic nanocomposites: mechanical properties", Curr. Op. Solid Sate Mater. Sci., 3, (1998), 490-495.

[17] Marshall D.B., Ritter J.E.: „Reliability of advanced structural ceramics and ceramic matrix composites - a review", Ceram. Bull., 66, (1987), 309-317.

[18] Kuntz J.D., Zhan G.D., Mukherjee A.K.: „Nanocrystalline-matrix ceramic composites for improved fracture toughness", MRS Bulletin, (2004), 22-27.

[19] French J.D., Chan H.M., Harmer M.P., Miller G.A.: „High-temperature fracture toughness of duplex microstructures", J. Am. Ceram. Soc., 79, (1996), 58-64.

[20] Wang H., Gao L., Shen Z., Nygren M.: „Mechanical properties of Al_2O_3-5 vol.% YAG composites", J. Eur. Ceram. Soc., 21, (2001), 779-783.

[21] Towata A., Hwang H.J., Yasuoka M., Sando M., Niihara K.: „Preparation of polycrystalline YAG/alumina composite fibers and YAG fiber by sol-gel metod", Composites A, 32, (2001), 1127-1131.

[22] Okada K., Motohashi T., Kameshima, Y. Yasumori A.: "Sol-gel synthesis of YAG/Al_2O_3 long fibres from water solvent system", J. Eur. Cer. Soc., 20, (2000), 561-567.

[23] Li W.Q., Gao L.: „Processing, microstructure and mechanical properties of 25 vol.% YAG-Al_2O_3 nanocomposites", Nanostruct. Mater., 11, (1999), 1073-1080.

[24] Wang H., Gao L.: „Preparation and microstructure of polycrystalline Al_2O_3-YAG composites", Ceram. Int., 27, (2001), 721-723.

[25] Palmero P., Simone A., Esnouf C., Fantozzi G., Montanaro L.: „Comparison Among Different Sintering Routes for Preparing Alumina-YAG Nanocomposites", J. Eur. Cer. Soc., 26, (2006), 941-947.

[26] Palmero P., Naglieri V., Chevalier J., Fantozzi G., Montanaro L.: „Alumina-based nanocomposites obtained by doping with inorganic salt solutions: Application to immiscible and reactive systems", J. Eur. Cer. Soc., 29, (2009), 59-66.

[27] http://www.taimei-chem.co.jp

[28] http://www.baikowski.com

[29] Anstis, G.R., Chantikul, P., Lawn, B.R., Marshall, D.B.: „A critical evaluation of indentation techniques for measuring techniques for measuring fracture toughness: I, direct crack measurements", J. Am. Ceram. Soc., 64, (1981), 533-538.

[30] Gao L., Shen Z., Miyamoto H., Nygren M.: „Superfast densification of axide-oxide ceramic composites", J. Am. Ceram. Soc., 82 (1999), 1061-1063.

[31] Hall E.O.: „The deformation and ageing of mild steel: III. Discussion of results", Proc. Phys. Soc., 64, (1951), 747-753.

♦

Received 29 April 2010; accepted 20 May 2010